

**NASA  
Technical  
Paper  
2092**

January 1983

NASA  
TP  
2092  
c.1

# Results From Tests, With Van-Mounted Sensor, of Magnetic Leader Cable for Aircraft Guidance During Roll-Out and Turnoff

James C. Young,  
W. Thomas Bundick,  
and Stewart H. Irwin



AFWL/SUL  
TECHNICAL LIBRARY  
KIRTLAND AFB, NM 87117

**NASA**

**NASA  
Technical  
Paper  
2092**

1983

TECH LIBRARY KAFB, NM



0134932

# Results From Tests, With Van-Mounted Sensor, of Magnetic Leader Cable for Aircraft Guidance During Roll-Out and Turnoff

James C. Young,  
W. Thomas Bundick,  
and Stewart H. Irwin  
*Langley Research Center  
Hampton, Virginia*

**NASA**

National Aeronautics  
and Space Administration

Scientific and Technical  
Information Branch



CONTENTS

SUMMARY . . . . . 1

INTRODUCTION . . . . . 1

SYMBOLS . . . . . 3

THEORY OF OPERATION . . . . . 5

DESCRIPTION OF EXPERIMENTAL EQUIPMENT AND PROCEDURES . . . . . 9

    Sensor . . . . . 10

    Instrumentation and Van Installation . . . . . 11

    Cable and Current Source . . . . . 13

    Tests With Van-Mounted Sensor . . . . . 14

    Tests With Aircraft-Mounted Sensor . . . . . 15

TEST RESULTS . . . . . 16

    Basic Measurements . . . . . 16

    Effect of Cable Loop Geometry . . . . . 19

    Effect of Runway Construction Material . . . . . 21

    Effect of Aircraft Structure . . . . . 23

    Effect of Electromagnetic Interference . . . . . 26

    Effect of Band-Pass Filter Phase Response on Synchronous Detector . . . . . 28

    Earth Return Tests . . . . . 29

    Bias and Noise Errors . . . . . 30

CONCLUDING REMARKS . . . . . 33

REFERENCES . . . . . 34



## SUMMARY

A magnetic leader cable laid along the path that an aircraft is intended to follow is a potential source of guidance information during roll-out, turnoff, and taxi. This report contains a description of a series of van tests conducted with such a system and a discussion of the results of these tests.

A breadboard experimental sensor and instrumentation were installed in a passenger van with the sensor coils mounted on a rig on the back of the van. Tests were conducted at the Wallops Flight Center, where a leader cable was temporarily installed at different locations on the taxiways and runways. Both static and dynamic data were taken to evaluate the capability of the system to measure lateral displacement from the cable and heading relative to the cable. Test variables included frequency of the current in the cable, van displacement, van heading, coil height, and runway construction material. Limited static test data were taken at the Langley Research Center with the coils mounted in the TCV Boeing 737 research aircraft.

Results of these tests show a good agreement between the theory of operation and the experimental data. The results indicate that a magnetic leader cable system is potentially usable as a sensor for measuring aircraft lateral displacement from runway and turnoff center line. The error in measuring displacement generally decreases nearer the cable, and close to the cable, accuracies of 0.1 or 0.2 m were achieved.

The magnetic field is distorted by the metal van or aircraft producing an error in the measurement of heading. Because of this effect the system may not be usable to measure heading.

The sensor was affected to various degrees by the runway construction material and by interference from other aircraft electrical systems. These interference effects were reduced by filtering in the sensor. The effects of van or aircraft metal, runway construction, and aircraft electrical systems were less when operating at a cable current of 150 Hz than they were at 990 Hz. In contrast, less cable current was required and the effect of a 60-Hz primary-power interference was less when operating at a cable current frequency of 990 Hz. Additional testing is required to determine the best operating frequency and to fully evaluate the system with the sensor installed in an aircraft.

## INTRODUCTION

The new Microwave Landing System (MLS) being developed by the Federal Aviation Administration is designed to provide sufficiently accurate guidance during final approach and touchdown to permit aircraft to land under conditions of severely reduced visibility. In addition, the azimuth and DME (distance measuring equipment) functions of the MLS will provide some guidance during roll-out under these same poor visibility conditions. On the other hand, guidance during turnoff and taxi is currently available only through visual means, and as such, it is inadequate during periods of extremely low visibility. Furthermore, the MLS, together with advanced avionics and air traffic control techniques, has the potential to increase runway capacity by decreasing the spacing between landing aircraft. Decreased landing intervals demand that runway occupancy time be decreased, that is, landing aircraft be cleared from

the runway rapidly. One technique for reducing runway occupancy time is the use of high-speed turnoffs. Safe and efficient use of high-speed turnoffs requires the availability of turnoff guidance, particularly for use with automatic controls. Clearly, if the MLS and high-speed turnoffs are to be used to their peak potential, appropriate guidance information during turnoff and taxi must be made available. One potential source of such guidance is the magnetic leader cable. The cable would be buried in the runway, turnoff, and taxiway along the path that the aircraft is to follow, as shown in figure 1. A sensor in the aircraft would detect signals from the cable and provide guidance to the pilot or automatic control system. The magnetic leader cable would supplement the MLS by providing an independent guidance signal during roll-out and by providing guidance during turnoff and taxi in areas of the airfield outside of MLS coverage.

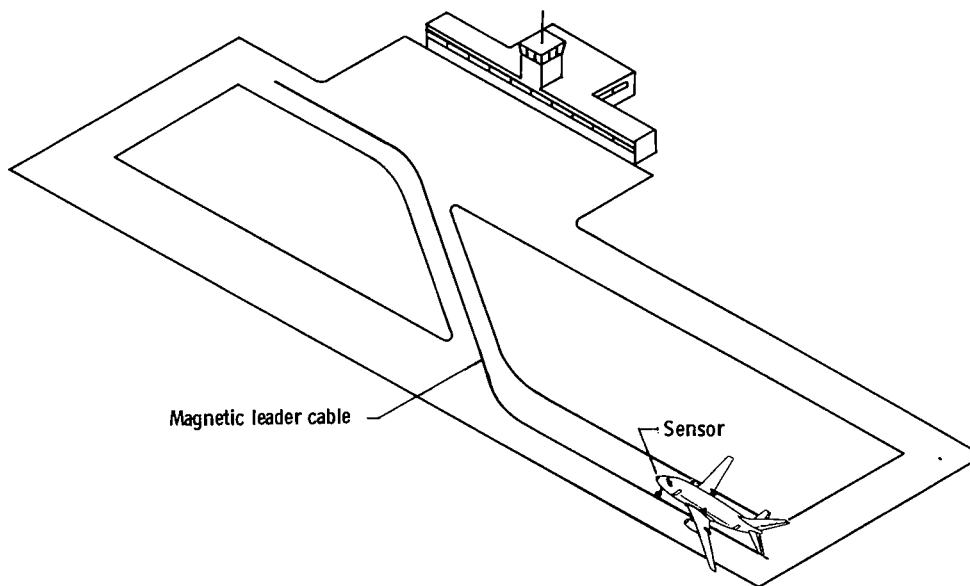


Figure 1.- Roll-out and turnoff guidance with magnetic leader cable.

The magnetic leader cable was investigated by the British (refs. 1 and 2) as early as the 1950's as a source of guidance during final approach and landing, but it was never adopted as an operational system. One factor limiting its usefulness in that application was the difficulty in obtaining accurate guidance during final approach. This limitation would not be a factor in the current concept because MLS guidance would be utilized during final approach, and the leader cable would not be used prior to touchdown.

Work on the magnetic leader cable has been revived as part of the NASA Terminal Configured Vehicle (TCV) program. One facet of this effort involves the investigation via computer simulation of aircraft performance during roll-out and turnoff using MLS and magnetic leader cable sensors. Portions of this work were performed under contract to NASA and have been reported in references 3 and 4.

A second facet of the effort is the development of the sensor system for the magnetic leader cable. One portion of this development is the theoretical analysis of the effects on sensor accuracy of aircraft attitude and cable geometry. This work

has been reported in detail in reference 5. The other portion of the development of the sensor system is the field testing of a set of experimental equipment with a sensor based on a design by Ohio State University; these tests are the subject of this report.

Tests were performed with a sensor mounted on a van, and the runways and taxiways at Wallops Flight Center were used to evaluate the basic accuracy of the experimental system. These tests included collecting data to determine the effects of taxiway turns and to determine the effects of runway construction material, such as asphalt and reinforced concrete. Additional tests were conducted to determine the effects of aircraft metallic structure on system performance and to determine if the system would be affected by electrical interference from other aircraft systems and from runway lights. This report contains a brief discussion of the theory of operation of the magnetic leader cable system, a description of the experimental equipment and procedures used to conduct each of these tests, and a comprehensive discussion of the results of each of these tests.

#### SYMBOLS

$A_x, A_y, A_z$	area of x-, y-, and z-coil, respectively, $m^2$
$\vec{B}$	magnetic induction field, $Wb/m^2$
$B_x, B_y, B_z$	Cartesian components of $\vec{B}$ , $Wb/m^2$
$\vec{d\ell}$	incremental length of current element in cable, m
$E_3$	peak value of voltage sine wave at synchronous detector in z-channel, V
$\vec{H}$	magnetic intensity, A/m
H	magnitude of $\vec{H}$ , A/m
$H_x, H_y, H_z$	Cartesian components of $\vec{H}$ , A/m
$I(t)$	time-varying current in cable, A
I	rms current in cable, A
$\vec{i}_\theta$	unit vector in $\theta$ -direction in cylindrical coordinates
$\hat{i}_1, \hat{i}_2, \hat{i}_3$	unit vector perpendicular to plane of x-, y-, and z-coil, respectively
$k_{y1}$	calibration factor relating estimate $\hat{y}_1$ to voltage ratio $V_3/V_2$ , m
$k_{y2}$	calibration factor relating estimate $\hat{y}_2$ to voltage ratio $V_3/(V_2^2 + V_3^2)$ , m
$k_\psi$	calibration factor relating estimate $\hat{\psi}$ to voltage ratio $V_1/V_2$ , m
$N_x, N_y, N_z$	number of turns in x-, y-, and z-coil, respectively
NA	coil gain when equal gain is assumed for all coils, $N_x A_x = N_y A_y = N_z A_z$ , $m^2$

$Q$	filter quality factor
$t$	time, sec
$V_x, V_y, V_z$	postdetection voltage in x-, y-, and z-channel, respectively, V
$V_{y1}, V_{y2}, V_\psi$	voltage at $\hat{y}_1$ , $\hat{y}_2$ , and $\hat{\psi}$ output, respectively, V
$V_{y1}^o$	static measured voltage at $\hat{y}_1$ output at point $y = y^o$ , V
$V_1, V_2, V_3$	rms voltage output of x-, y-, and z-coil, respectively, V
$v_o$	synchronous detector output, V
$v_2(t), v_3(t)$	time-varying voltages at synchronous detectors in z-channel, V
$x, y, z$	Cartesian coordinates
$y^o$	lateral displacement at which a particular static measurement was made, m
$\hat{y}_1, \hat{y}_2$	estimate of coil displacement from cable defined by equation (6) or (7c), respectively, m
$z$	height of coil, m
$\beta$	relative phase between voltages at z-channel synchronous detector input, rad
$\epsilon_{y1}, \epsilon_{y2}$	residual from least-squares polynomial fit to static data in $\hat{y}_1$ and $\hat{y}_2$ output, respectively, m
$\theta$	angular coordinate in cylindrical coordinates, rad
$\mu_o$	permeability of free space, $4\pi \times 10^{-7}$ , Wb/A-m
$\rho$	radial coordinate in cylindrical coordinates, m
$\sigma_{y1}$	sample standard deviation of $\hat{y}_1$ data, m
$\psi$	aircraft heading relative to cable (equivalent to yaw during roll-out), rad or deg
$\hat{\psi}$	estimate of $\psi$ defined by equation (10b), rad or deg
$\omega$	angular frequency of current in cable, rad/sec

Abbreviations:

AC	asphaltic concrete
AM	amplitude modulation
APU	auxiliary power unit

ac	alternating current
amp	amplifier
BPF	band-pass filter
DVM	digital voltmeter
dc	direct current
det	detector
elect	electronics
gen	generator
limit	limiter
PCC	portland cement concrete
R/W	runway
rms	root mean square
synch	synchronous
T/W	taxiway

#### THEORY OF OPERATION

A detailed development of the theory of the magnetic leader cable is contained in reference 5, and only a brief discussion is presented herein. Consider an infinitely long, straight conductor coincident with the x-axis carrying a current  $I(t)$ , as depicted in figure 2. The magnetic leader cable utilizes a sinusoidal current in the audio frequency range, say 100 Hz to 2500 Hz. Because of the extremely long wavelengths (greater than 100 km) and short distances (less than 5 km) involved, the propagation time can be neglected. Thus, to simplify the mathematics, the time dependence of the current and resulting magnetic field is omitted.

Returning now to figure 2, the magnetic intensity  $\vec{H}$  at a point  $P(x,y,z)$  can be computed with Ampere's circuital law as follows:

$$\int_C \vec{H} \cdot d\vec{\ell} = I \quad (1)$$

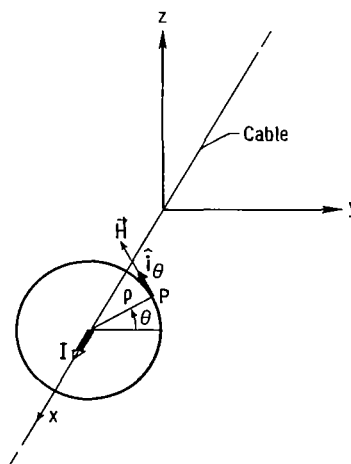


Figure 2.- Geometry for infinite straight cable.

where

$\vec{H}$  magnetic intensity  
 $d\vec{\ell}$  incremental length of current element in cable  
I rms current in cable

Because the field is symmetrical about the conductor and is everywhere in the  $\theta$ -direction, equation (1) can be solved to give

$$\vec{H} = \frac{I}{2\pi\rho} \hat{i}_\theta \quad (2)$$

where

$\rho$  radial coordinate  
 $\hat{i}_\theta$  unit vector in  $\theta$ -direction

In Cartesian coordinates, equation (2) becomes

$$H_x = 0 \quad (3a)$$

$$H_y = -H \sin \theta = -\frac{I}{2\pi} \frac{z}{y^2 + z^2} \quad (3b)$$

$$H_z = H \cos \theta = \frac{I}{2\pi} \frac{y}{y^2 + z^2} \quad (3c)$$

where

H magnitude of  $\vec{H}$   
 $H_x, H_y, H_z$  Cartesian components of  $\vec{H}$   
 $x, y, z$  Cartesian coordinates

Suppose there were three mutually orthogonal coils located at point P such that the axes  $\hat{i}_1$ ,  $\hat{i}_2$ , and  $\hat{i}_3$  of the coils were parallel to the coordinate axes  $x$ ,  $y$ , and  $z$ , respectively. The magnitude of the voltage  $V_1$ , induced in the x-coil by the magnetic field  $\vec{B}$  is

$$V_1 = \omega N_x A_x B_x \quad (4)$$

where

$\omega$  angular frequency of current in cable, rad/sec  
 $N_x$  number of turns in x-coil

$A_x$  cross-sectional area of x-coil  
 $B_x$  x-component of magnetic field  $\vec{B}$   
 $\vec{B} = \mu_0 \vec{H}$   
 $\mu_0 = 4\pi \times 10^7 \text{ Wb/A}$

The velocity-induced voltage in the coil can be neglected because it is usually small relative to  $V_1$  and because it is largely eliminated by the band-pass filters.

Combining equations (3a) and (4) gives

$$V_1 = 0 \quad (5a)$$

Similarly for the y- and z-coils,

$$V_2 = \omega N_y A_y B_y = \frac{-\mu_0 \omega N_y A_y I}{2\pi} \frac{z}{y^2 + z^2} \quad (5b)$$

and

$$V_3 = \omega N_z A_z B_z = \frac{\mu_0 \omega N_z A_z I}{2\pi} \frac{y}{y^2 + z^2} \quad (5c)$$

where

$N_y, N_z$  number of turns in y- and z-coil, respectively  
 $A_y, A_z$  cross-sectional area of y- and z-coil, respectively  
 $B_y, B_z$  y- and z-component, respectively, of magnetic field  $\vec{B}$

Take the ratio of the voltages  $V_3$  to  $V_2$ , solve for  $y$ , and denote this solution by  $\hat{y}_1$  to get

$$\hat{y}_1 = - \frac{N_y A_y}{N_z A_z} \frac{z V_3}{V_2} = k_{y1} \frac{V_3}{V_2} \quad (6)$$

where  $k_{y1}$  is a calibration factor. The coil constants  $N_y$ ,  $A_y$ ,  $N_z$ , and  $A_z$  are known or can be calibrated. If the height  $z$  of the coils is known, the calibration factor  $k_{y1}$  can be calculated or measured. Then by measuring the coil voltages  $V_2$  and  $V_3$  and using equation (6), an estimate of the displacement  $y$  of the coils from the magnetic leader cable can be determined. Note that the estimate  $\hat{y}_1$  is a linear function of the ratio of voltages  $V_3/V_2$ .

If the gains of the coils are equal, the displacement  $y$  can also be determined via an alternative technique that requires a knowledge of the current  $I$  in the cable but does not require that the height  $z$  be known. This can be seen by finding the ratio  $V_3 / (V_2^2 + V_3^2)$  as follows:

$$\frac{V_3}{V_2^2 + V_3^2} = \frac{2\pi N_z A_z}{\mu_o \omega I} \frac{y(z^2 + y^2)}{(N_z^2 A_z^2 z^2 + N_y^2 A_y^2 y^2)} \quad (7)$$

Now, if  $N_y A_y = N_z A_z$ , equation (7) becomes

$$\frac{V_3}{V_2^2 + V_3^2} = \frac{2\pi y}{\mu_o \omega I N_y A_y} \quad (8)$$

Equation (8) can be solved for  $y$  to obtain the following equation with  $y$  being denoted  $\hat{Y}_2$ :

$$\hat{Y}_2 = \frac{\mu_o \omega I N_y A_y}{2\pi} \frac{V_3}{V_2^2 + V_3^2} = k_{Y2} \frac{V_3}{V_2^2 + V_3^2} \quad (9)$$

where  $k_{Y2}$  is a calibration factor. Note that in this expression  $\hat{Y}_2$  is a linear function of the ratio  $V_3/(V_2^2 + V_3^2)$ .

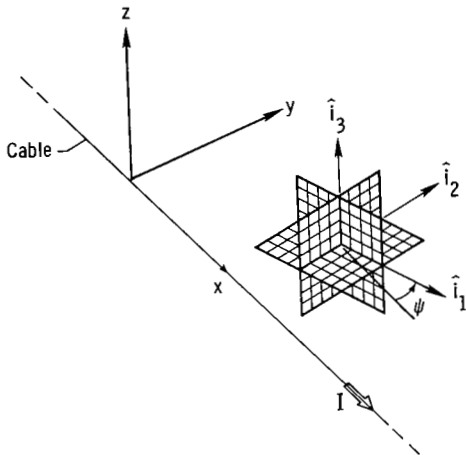


Figure 3.- Coil geometry.

Suppose now that the coils are rotated in the  $xy$ -plane such that  $\hat{i}_1$  makes an angle  $\psi$  with the  $x$ -axis, as shown in figure 3. Now the voltage output  $V_3$  of the  $z$ -coil remains the same, but the voltages  $V_1$  and  $V_2$  become (since  $B_x = 0$ )

$$V_1 = \omega N_x A_x B_y \sin \psi \quad (10a)$$

$$V_2 = \omega N_y A_y B_y \cos \psi \quad (10b)$$

where  $\psi$  is aircraft heading. Taking the ratio  $V_1/V_2$  gives

$$\frac{V_1}{V_2} = \frac{N_x A_x}{N_y A_y} \tan \psi \quad (11)$$

If the angle  $\psi$  is small, equation (11) can be approximated by

$$\frac{V_1}{V_2} \approx \frac{N_x A_x \psi}{N_y A_y} \quad (12a)$$

which can be solved for  $\psi$  to yield

$$\hat{\psi} \approx \frac{N_Y A_Y}{N_X A_X} \frac{V_1}{V_2} = k_\psi \frac{V_1}{V_2} \quad (12b)$$

Note that in this equation the estimate  $\hat{\psi}$  is a linear function of the ratio  $V_1/V_2$ . Equation (6) for the displacement now becomes

$$\hat{Y}_1 = - \frac{N_Y A_Y}{N_Z A_Z} z \cos \psi \frac{V_3}{V_2} \quad (13)$$

However, if  $\psi$  is small, equation (13) can be approximated by equation (6).

We have shown conceptually that for an infinitely long straight cable carrying a current  $I$ , the lateral displacement  $y$  (relative to the cable) of a set of three mutually orthogonal coils can be determined by measuring the voltage output of the appropriate coils and processing these measurements with either of two algorithms. The use of one algorithm requires that the height of the coils be known, whereas use of the other algorithm requires that the magnitude of the current in the cable be known. Furthermore, the angle of rotation of the coil in the  $xy$ -plane can be determined by using the coil voltages and processing them with a third algorithm. Conceptually it follows that, if the coils are rigidly attached to an aircraft and the magnetic cable is laid on the runway center line, the sensor can be used to measure displacement of the aircraft from center line and heading of the aircraft relative to center line.

An experimental sensor system was designed to measure displacement and heading according to equations (6), (7), (8), (9), and (12). It has been shown theoretically in reference 5 and it can be seen from the results of field tests of the experimental sensor that the calibration factors  $k_{y1}$ ,  $k_{y2}$ , and  $k_\psi$  are not constants for a realistic magnetic leader cable system. Rather they are variables which depend on the geometry of the cable, runway construction material, aircraft structure, and other effects. These factors have been measured experimentally under various conditions, and the effect on sensor accuracy investigated.

#### DESCRIPTION OF EXPERIMENTAL EQUIPMENT AND PROCEDURES

This section contains a brief description of the magnetic leader cable sensor used in both the van tests and the very limited aircraft tests and a discussion of how the sensor was mounted in the test van and of the associated instrumentation. This section also contains a description of the temporary cable installations at Wallops Flight Center, including the current source, that is, the source of ac current for the cable. The remainder of this section contains a discussion of the procedures used in conducting the van tests and the aircraft tests.

## Sensor

A block diagram of the sensor is shown in figure 4. In the experimental system all elements of the sensor were implement in analog form.

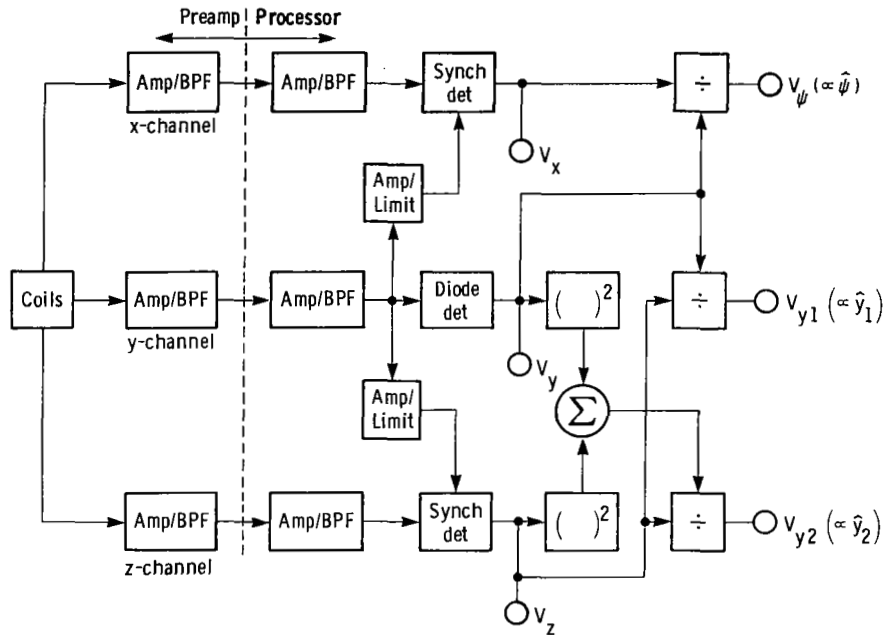


Figure 4.- Block diagram of experimental sensor.

The experimental sensor consisted of a set of coils, a preamplifier, and a processor. The three coils were wound with orthogonal axes on a 10-cm (4-in.) wooden cube using AWG no. 28 wire. The coils had between 215 and 400 turns each with the exact number of turns in each coil calculated to produce a constant product of turns times the coil area.

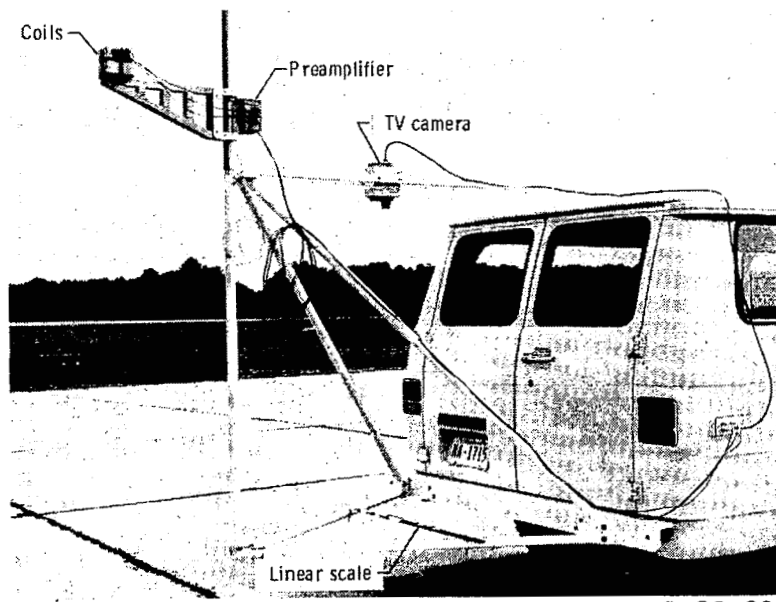
The preamplifier consisted of three identical channels, x, y, and z, each with a low noise input amplifier and a one pole-pair amplifier/band-pass filter. The passive components of the filters were mounted on plug-in modules to facilitate changing frequency and bandwidth. The outputs of the preamplifier were fed through coaxial cables to the processor for additional signal conditioning and processing.

In the processor, the signals in the three channels were amplified and filtered again in an amplifier/band-pass filter identical to the one in the preamplifier. The filters in the processor also utilized plug-in modules. These signals are ac signals at the cable current frequency (150, 165, or 990 Hz). After amplification and filtering, the signals are detected by half-wave rectifiers and filtered to produce three dc signals,  $V_x$ ,  $V_y$ , and  $V_z$ , each proportional to one component of the magnetic field surrounding the coils, as in equations (5) and (10). These dc signals,  $V_x$ ,  $V_y$ , and  $V_z$ , are actually slowly varying dc signals proportional to the amplitudes of the ac signals  $V_1$ ,  $V_2$ , and  $V_3$ , respectively, in the x-, y-, and z-channels. These ac signal amplitudes vary with position and heading. The rectifiers in the x- and z-channels are synchronous detectors driven by the signal in the y-channel; thus, the relative algebraic signs of the signals are retained.

These dc signals are now processed in analog function circuits to produce three output signals:  $V_{\psi}$ , which is proportional to heading relative to the cable, and  $V_{y1}$  and  $V_{y2}$ , which are proportional to lateral displacement from the cable. Since the relative algebraic signs of the input signals have been retained, the signs of the output signals indicate the directions of the heading and displacement.

### Instrumentation and Van Installation

For ease and economy of testing, the experimental sensor along with support equipment was installed in a passenger van modified for this use. An aluminum structure, shown in figure 5, was attached to the rear of the van to support the coils and preamplifier. The structure was designed both to allow some distance between the coils and the metal van and to allow adjustment in coil height.



L-82-205

Figure 5.- Van support structure with coils and preamplifier.

The signals  $V_x$ ,  $V_y$ ,  $V_z$ ,  $V_{y1}$ ,  $V_{y2}$ , and  $V_{\psi}$  were recorded on two 4-track analog tape recorders for posttest data analysis. A time code generator supplied a time code signal to each of the magnetic tape recorders for use in posttest data reduction. Any two of these signals (except time code) were recorded on a paper chart recorder for quick-look analysis. Each of these signals could be selected for display on a digital voltmeter for hand recording of static data.

A television camera was mounted on the coil support structure as seen in figure 5. The camera was used to televise a linear scale mounted on the support structure and a rope marker laid on the runway. The rope was laid along the path that the van was to follow. The picture was fed to a television monitor to assist in positioning the van for static tests and to assist in driving the desired path. The video was also recorded on magnetic tape for posttest data analysis.

Power was supplied to the sensor and the instrumentation by a 500-W, 110-V ac inverter operating off the van 12-V battery/alternator system. A block diagram of the instrumentation is shown in figure 6, and a photograph of the rack inside the van is in figure 7.

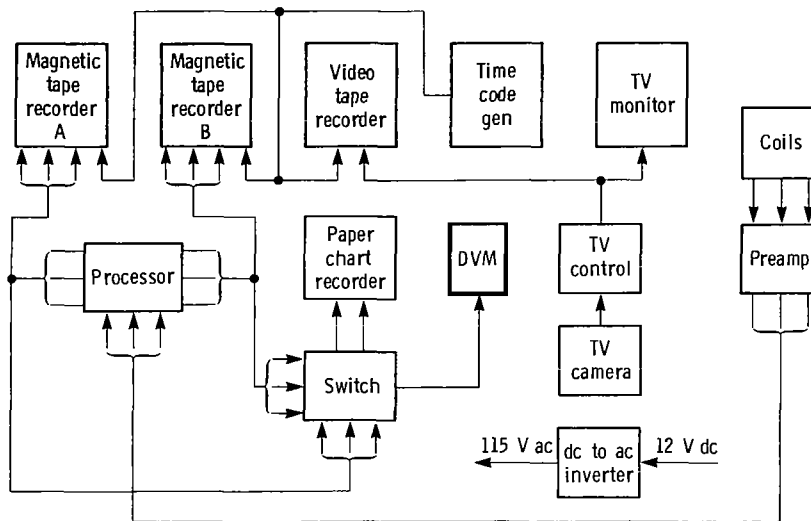
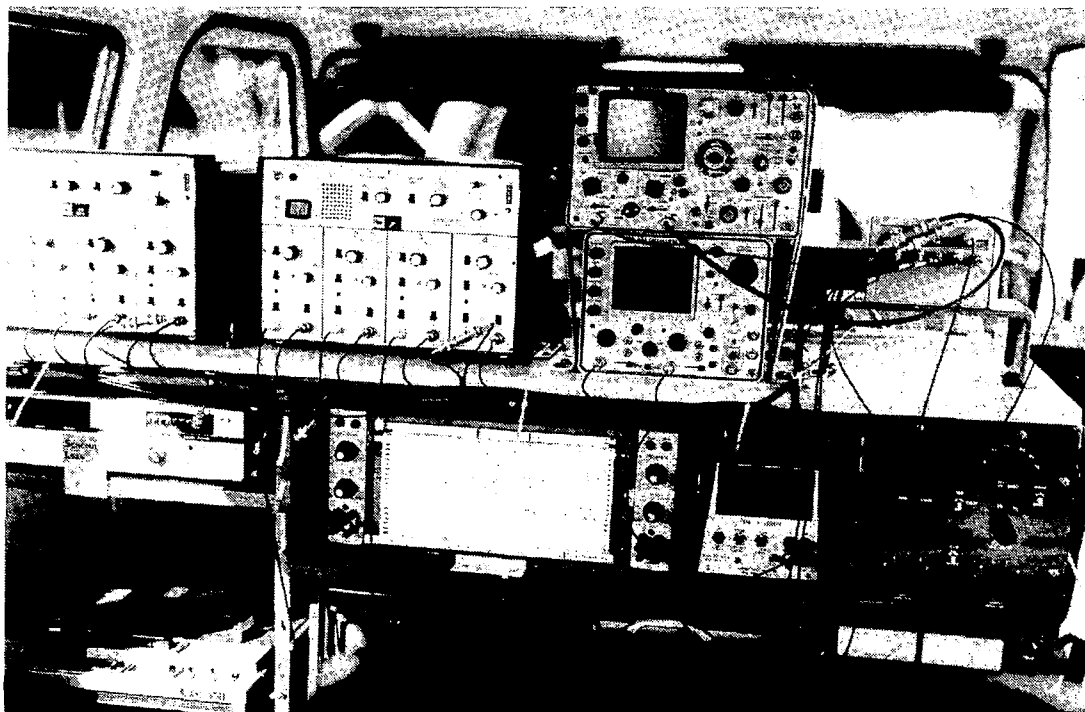


Figure 6.- Block diagram of van instrumentation.



L-79-7941

Figure 7.- Instrumentation rack in test van.

## Cable and Current Source

The leader cable was simply a length of AWG no. 14 or AWG no. 16 insulated, stranded wire laid along the center line of the taxiway or runway. It was held in place by long staples in the tar between sections of concrete and by bags of lead shot weighing approximately 1.3 kg (3 lb). These bags were sufficiently small that no effect on the magnetic field could be detected with the experimental system. To provide a return path for the current, the wire was laid in the shape of a rectangle with the other three sides in the grassy area between the runway and taxiway. Figure 8 illustrates a typical installation.

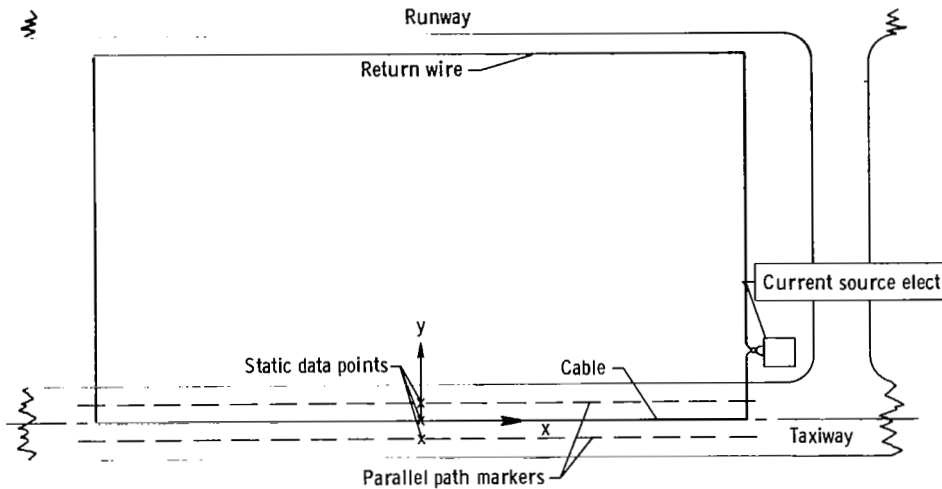


Figure 8.- Typical test site layout.

Current for the cable was supplied by a laboratory-type signal generator driving an audio power amplifier capable of supplying 600 W into an 8-Ω load. A counter and an ammeter were required to set the frequency and magnitude of the cable current. The current source and other instrumentation were located along the rectangular loop as close as possible to a source of 110-V ac power.

In order to examine the effects of different types of runway construction material and the effects of a curved path on system performance, the cable was laid at the various test sites at Wallops Flight Center listed in table I and identified by

TABLE I.- TEST SITES AT WALLOPS FLIGHT CENTER

Location	Size, m	Cable geometry in test area	Runway/taxiway material in test area
Taxiway 10/28	116 by 306	Straight	Concrete
Runway 10/28	116 by 546	Straight	Part concrete, part asphalt
Taxiway 04/22	116 by 306	Straight	Asphalt
Taxiway 04/22	116 by 549	Straight	Part concrete, part asphalt
Taxiway 04/22	<sup>a</sup> 116 by 550	S-curve	Part asphalt, part asphalt over concrete

<sup>a</sup>67 m wide at narrow end.

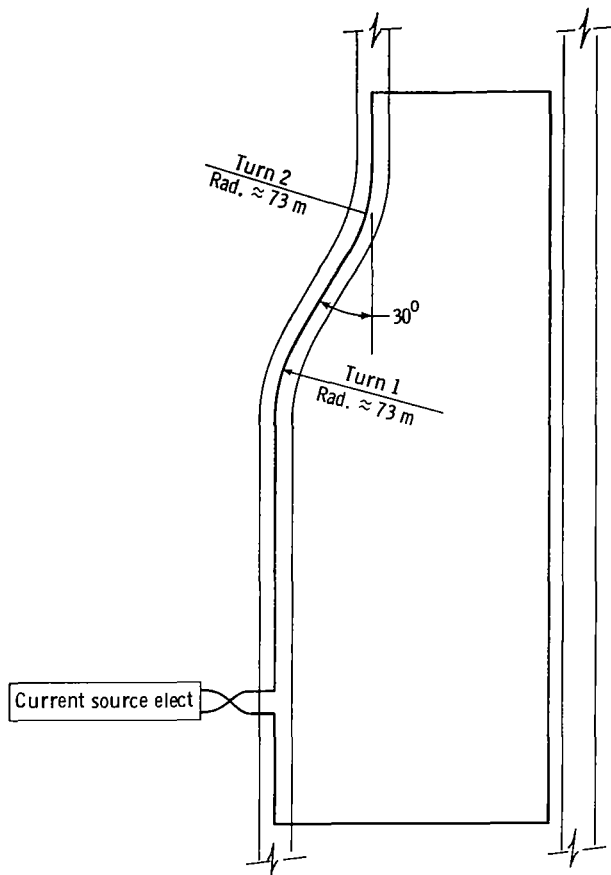


Figure 9.- Cable installation on taxiway 04/22 curve.

(4 to 12 ft) with most data taken at 2.4 m (8 ft), which is approximately the height at which a coil might be mounted in the nose of a 737 aircraft.

For the dynamic tests the van was driven along the desired path at speeds of approximately 3.6, 8.9, or 22.4 m/sec (8, 20, or 50 mph), with most of the runs being made at 8.9 m/sec. While 8.9 m/sec was somewhat arbitrary, it did afford a compromise among realistic aircraft speed, ability to accurately drive the path, and a desirable data record length in terms of time. Most paths were parallel to the cable at displacements from the cable of as much as 21.3 m (70 ft). These paths were marked by the tar between the concrete sections and by existing painted lines on the runway or taxiway where these were available at the proper displacement. Otherwise, a small diameter yellow rope, held in place by staples and bags of shot, was used as a marker.

The test procedure for each parallel run normally consisted first of recording static data with the vehicle aligned with the proper parallel mark and at the center of the test area. Then dynamic data were recorded while the van was driven along the selected parallel marker at a constant speed. In a test sequence, several runs were made at increasing lateral displacements, and complementary runs were made on the opposite side of the center line.

the runway or taxiway numbers. The construction materials at these sites include concrete, asphaltic concrete, and asphalt over concrete. Figure 9 illustrates the curved path installation on taxiway 04/22. This path geometry is representative of the turns that would be present in a high-speed runway exit, although the turn radii in a high-speed exit probably would be larger.

#### Tests With Van-Mounted Sensor

In general, two types of tests were conducted: static tests, during which the van was stopped at a specified point, and dynamic tests, during which the van was driven along a desired path. For both types of tests, cable current frequencies of 150 Hz, 165 Hz, and 990 Hz were employed. The Ohio State University sensor was designed for a cable current frequency of 990 Hz, and the British had used 165 Hz. The cable current frequency of 150 Hz was used because it is farther from the primary-power third harmonic (180 Hz) than 165 Hz. The reason for this use is discussed later in the section "Test Results." Currents from 0.25 to 2.0 A were employed in the cable to obtain usable signal levels in the processor. Coil heights varied from 1.2 to 3.7 m

For the parallel paths, the van heading relative to the cable was always zero. For test at other headings, rope markers were laid at angles of  $5^{\circ}$ ,  $10^{\circ}$ , and  $15^{\circ}$  with respect to the cable. Static and dynamic data were taken along these paths in the same manner as along the parallel paths.

In the tests previously discussed, the leader cable was a complete rectangular loop of wire laid with one side on the runway or taxiway and with the ends and the other side on the adjacent grassy area, as shown in figure 8. Consideration was also given to the use of the earth as the return path for the cable current. This test layout, shown in figure 10, consisted of four ground rods, 2.4 m (8 ft) long, installed 30 m (100 ft) from the center line of the taxiway and 306 m (1005 ft) apart. The magnetic leader cable was electrically attached to the rods by the use of a wire tee at each end of the test site. The impedance of this system was measured at two frequencies. Static data were taken for the ground return configuration and compared with the rectangular loop data taken at the same site.

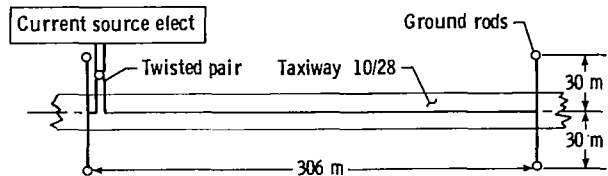


Figure 10.- Cable layout for earth return tests.

#### Tests With Aircraft-Mounted Sensor

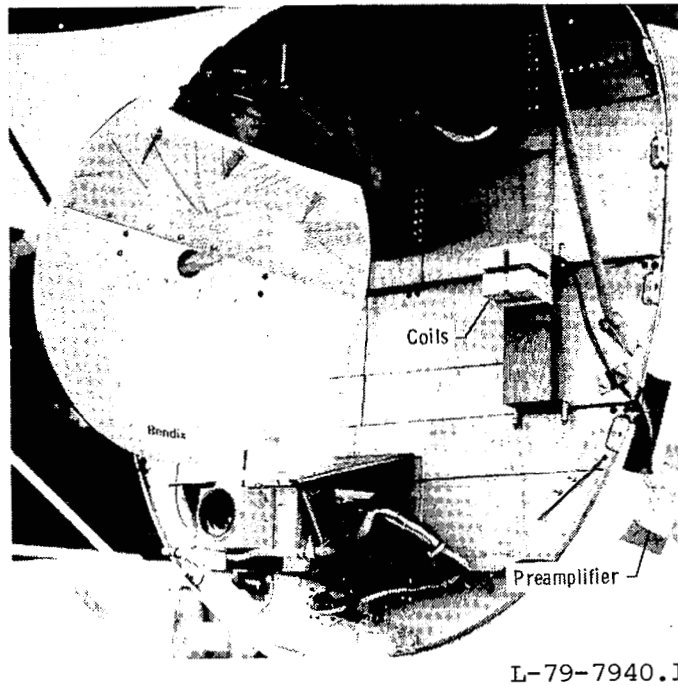
To obtain some preliminary data on both the effect of the metal aircraft structure and the effect of aircraft electrical systems on sensor performance, limited static tests were conducted with the TCV Boeing 737 aircraft. A magnetic leader cable loop was set up on a taxiway in front of the NASA hangar at the Langley Research Center. Static data were taken just as in the van tests with the following two exceptions: (1) the coils and preamplifier were removed from the van support structure and temporarily installed in one of two locations in the 737, and (2) the preamplifier was connected via extended cables to the processor and instrumentation in the van. One of the coil locations was inside the nose cone at a height of about 2.4 m (8 ft), and the other location was below the nose-wheel well at a height of 0.9 m (3 ft). The overall installation can be seen in the photograph in figure 11,



L-79-7939

Figure 11.- Experimental setup for aircraft tests.

and the nose-cone installation is shown in figure 12. The aircraft was positioned at the test point with a tug, and power to the aircraft electrical systems was supplied by the aircraft auxiliary power unit.



L-79-7940.1  
Figure 12.- Experimental coil installation in Boeing 737 nose cone.

#### TEST RESULTS

Discussed in this section are the results of tests conducted with the experimental equipment previously described. Considerably more data resulted from the measurements and data analysis than can be presented herein. However, a representative cross section of the data supporting all significant results and conclusions is included.

#### Basic Measurements

First consider a set of measurements taken to verify the basic relationships of equations (5) through (9) and to determine experimentally the calibration factors  $k_{y1}$  and  $k_{y2}$ . The postdetection dc voltages  $V_y$  and  $V_z$  are plotted in figure 13 as functions of  $y$ , the perpendicular displacement from the cable across the taxiway. Static measurements of  $V_y$  and  $V_z$  taken with the van-mounted equipment on taxiway 04/22 near the center of the cable ( $x \approx 0$ ) are shown. The current in the cable was 0.25 A at a frequency of 990 Hz. Also shown are theoretical values for the same quantities calculated with equations (5) as modified to include the gains of the electronics between coil output and the postdetection dc output. Measured gains of the electronics, computed gains ( $\omega NA$ ) of the coils, and theoretical values for the magnetic fields were used. The theoretical curves for the magnetic field amplitude were computed from theoretical expressions similar to equations (3) but derived for a

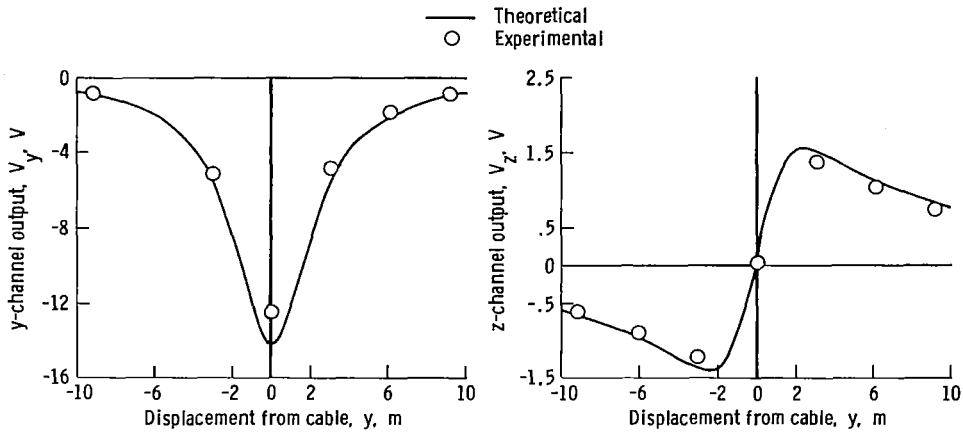


Figure 13.- Comparison of theoretical and experimental signal amplitudes.

closed rectangular loop (ref. 5) rather than an infinite straight wire. As can be seen from figure 13, the theoretical and experimental data agree quite well.

In figure 14, the measured  $\hat{y}_1$  and  $\hat{y}_2$  outputs  $V_{y1}$  and  $V_{y2}$  are plotted as functions of  $y$  taken at the same time as the data in figure 13. The  $\hat{y}_1$  data in figure 14(a) exhibit a slight nonlinearity not predicted by equation (6). A deviation from linearity is caused by the magnetic field produced by the other side of the rectangular loop as shown by the analysis of a rectangular loop in reference 5. The  $\hat{y}_2$  data in figure 14(b) also exhibit a nonlinearity, but it is less pronounced than that of  $\hat{y}_1$ .

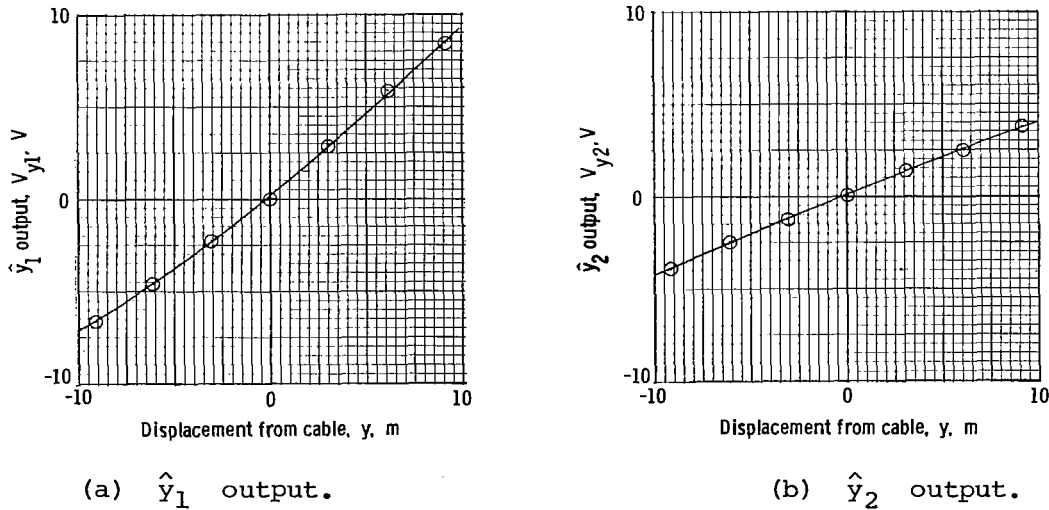


Figure 14.- Calibration curves for  $\hat{y}_1$  and  $\hat{y}_2$  from static data.

The data presented thus far were taken with the van and x-coil axis parallel to the cable; that is,  $\psi = 0^\circ$ . To determine the behavior of the estimate  $\hat{\psi}$ , measurements of  $V_\psi$  were made at several values of  $\psi$  and of  $y$ . These measurements were repeated at the same values of  $\psi$  and  $y$  but with the van headed in the opposite direction. It is recognized that  $\psi = 15^\circ$  represents an extreme value for heading for an aircraft in roll-out. However, the objective was to take measurements over a range of  $\psi$  to test the consistency of the data under the constraints of the accuracy with which the van and coils could be readily aligned in heading.

The  $\hat{\psi}$  output  $V_\psi$  is plotted as a function of  $y$  in figure 15(a) for nominal values of  $\psi$  of  $5^\circ$ ,  $10^\circ$ , and  $15^\circ$  with a cable current frequency of 990 Hz. According to equation (12b) for a given value of  $\psi$ ,  $V_\psi$  should not change as a function of  $y$ . In figure 15(a), however, it can be seen that whereas  $V_\psi$  is relatively constant on one side of the cable, it is a strong function of  $y$  on the other side. When headed in the opposite direction, the trend reverses. Thus, the measured output  $V_\psi$  was a function of  $y$  when the front of the van was slightly closer to the cable than were the coils. This behavior was consistent for all values of  $\psi$  used. (Note that positive  $y$  is always on the side of the cable towards the return wire and is independent of van direction.) Similar data are plotted in figure 15(b) for a cable current frequency of 165 Hz. For this frequency, the data exhibit very little dependence on  $y$ .

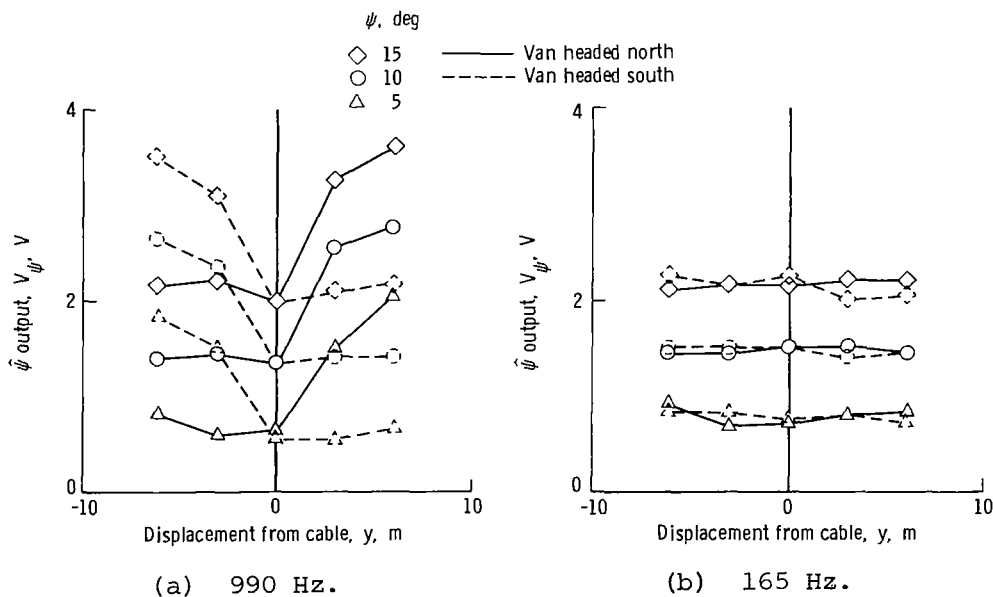


Figure 15.- Static calibration data for  $\hat{\psi}$  output.

The anomalies in the  $V_\psi$  data at 990 Hz appear to be caused by distortion of the magnetic field by the van and coil support structure. This behavior raised questions about the accuracy that could be obtained with the sensor mounted inside a metal aircraft; as a result a number of further tests were conducted to investigate the effects of a metal aircraft. These tests and the results are discussed later in a separate section.

The data presented in figures 13 through 15 were taken with the coil at a height of 2.4 m (8 ft). In figure 16, the effects of coil height on the  $\hat{y}_1$  and  $\hat{y}_2$  outputs can be seen. Figure 16(a) shows that the  $\hat{y}_1$  output voltage is a function of  $z$ , as predicted by equation (6). The  $\hat{y}_2$  output, on the other hand, is relatively constant for varying  $z$ , as predicted by equations (7) to (9). All data in figures 13 through 16 were taken with 0.25 A of 990-Hz current in the cable with the exception of figure 15(b).

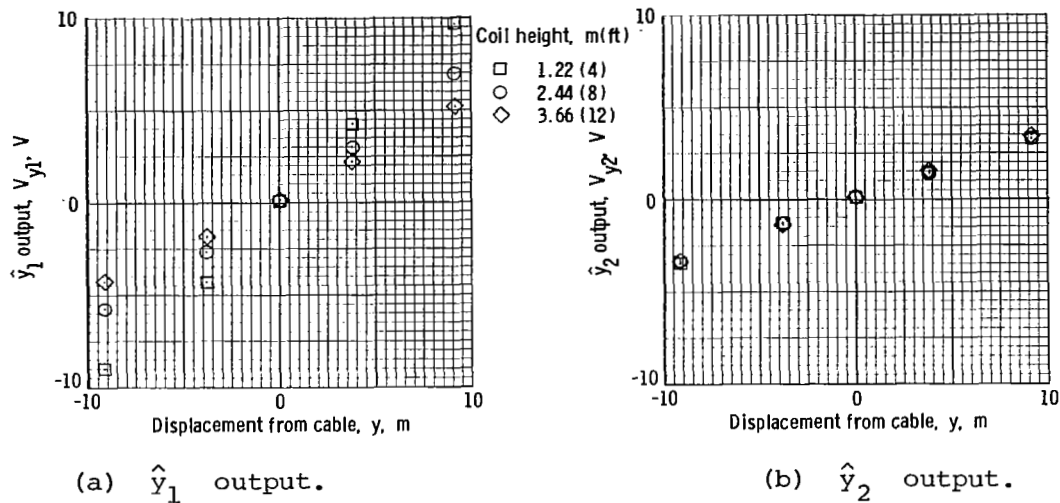


Figure 16.- Calibration curves for  $\hat{y}_1$  and  $\hat{y}_2$  at different coil heights.

#### Effect of Cable Loop Geometry

The  $\hat{y}_1$  and  $\hat{y}_2$  calibration curves in figure 14 have shown that the magnetic field from the return side of the loop causes the calibration curves to be nonlinear functions of  $y$ . If the loop return were closer than the 116 m (380 ft) used in taking the data for figure 14, the nonlinearity would be more pronounced. This effect is discussed in more detail in reference 5. In a similar manner, the current in the ends of the loop contributes to the field and produces changes in the sensor outputs. The effect can be seen in the time histories of the dynamic data; a typical time history is shown in figure 17. These data were taken at a van speed of approximately 8.9 m/sec (20 mph). From figure 17, it is obvious that the accuracy of the  $\hat{y}_1$  and  $\hat{\psi}$  outputs deteriorates rapidly near the ends of the loop. The variations in  $\hat{\psi}$  data away from the ends are apparently caused by the steel reinforcement in the concrete and are discussed later in the report.

The rectangular loop is configured to provide guidance in a straight line by using one side of the rectangle, such as along the runway center line during roll-out. To provide guidance during turnoff and taxi requires that the cable be laid along the path which the aircraft is to follow; thus, the loop is no longer rectangular. The errors introduced by the turns in the cable are theoretically examined in reference 5,

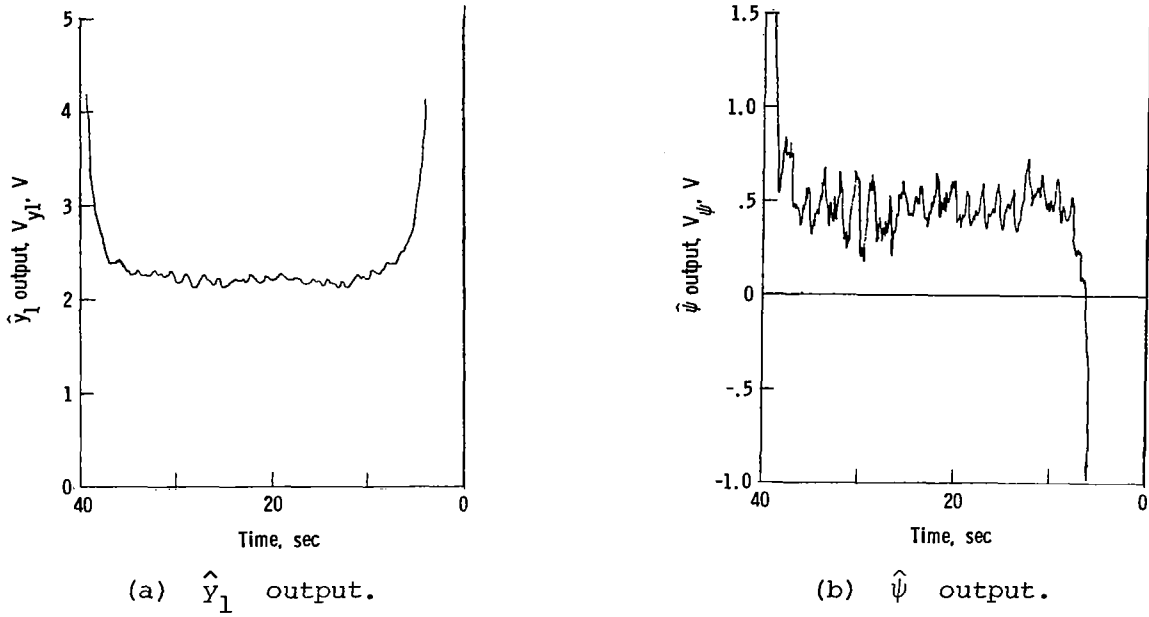
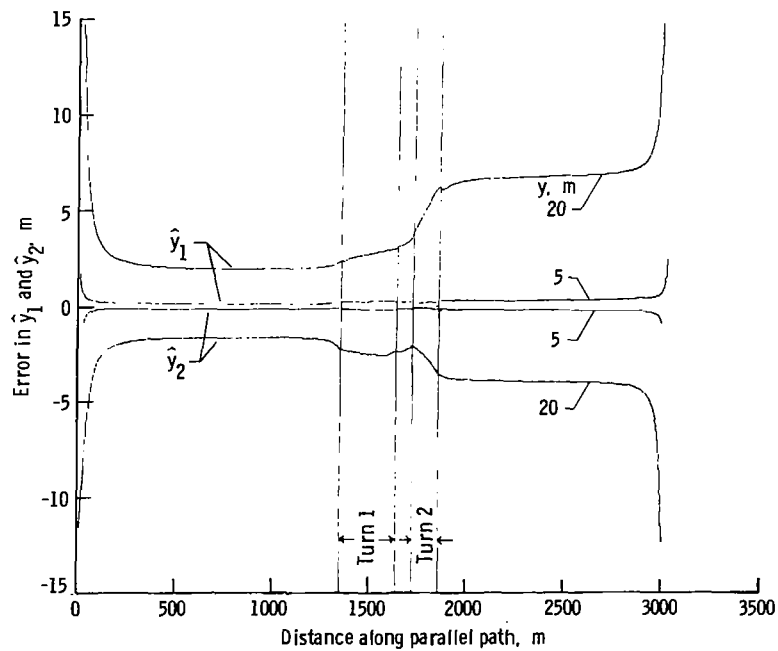


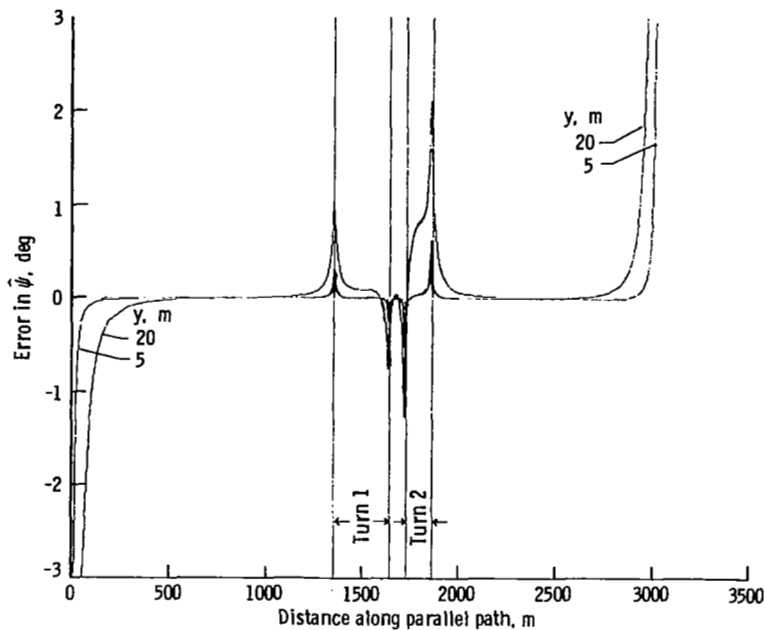
Figure 17.- Time histories of sensor outputs showing effects of ends of loops.

and a typical set of these results is plotted in figure 18. The theoretical bias-type errors are errors introduced by the loop when a linear calibration is assumed. Part of the error in  $\hat{y}_1$  and  $\hat{y}_2$  could be eliminated by using a nonlinear calibration as with a rectangular loop. Note that the error in  $\hat{y}_1$  and  $\hat{y}_2$  changes



(a) Error in estimates  $\hat{y}_1$  and  $\hat{y}_2$ .

Figure 18.- Errors due to turnoff geometry.



(b) Error in estimate  $\hat{\psi}$ .

Figure 18.- Concluded.

smoothly in the turns, and especially note that the error decreases as  $y$  approaches zero; that is, the error is small near the desired path. For  $\hat{\psi}$ , the error is relatively large at the beginning and end of the turns. The effect of these errors on automatic roll-out and turnoff performance will be determined by further simulation and testing. It may be that nonlinear calibration curves will not be required.

In figure 19, time histories of the sensor output signals are plotted for a typical data collection run around the turns on taxiway 04/22 at Wallops. (See fig. 9.) The output voltages have been converted to engineering units using a single-point calibration measurement at the intended path of  $y = -7.7$  m. The data, particularly  $V_{\psi}$ , can be seen to deviate in the first turn at around 37 sec. The deviation in the second turn at around 45 sec is not nearly as noticeable. Because of the difficulty in driving around the turns and keeping the coils accurately positioned, these data can only be used as a gross indicator of performance. From this viewpoint, the data, especially  $\hat{y}_1$  and  $\hat{y}_2$ , look sufficiently promising to warrant further experimentation. Moreover, comparison of the measured data and theoretical data throughout this section has confirmed the salient features of the concept.

#### Effect of Runway Construction Material

Runways at Wallops are constructed primarily with two types of material: portland cement concrete (PCC) and asphaltic concrete (AC). The PCC type of construction uses steel reinforcing mesh over the entire area and heavy steel dowel bars at selected joint locations. The steel in the PCC can distort the magnetic field and affect the signals used by the processor. The AC type of construction does not use reinforcing material; therefore, the magnetic field is not subject to the same distortion as with the PCC.

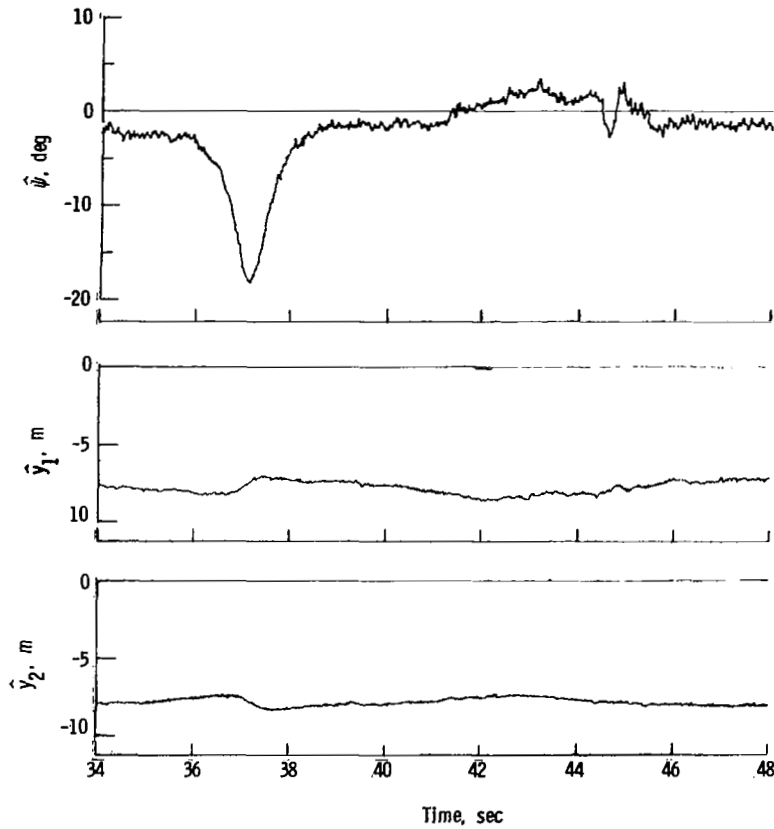


Figure 19.- Time history of sensor output data during turnoff.

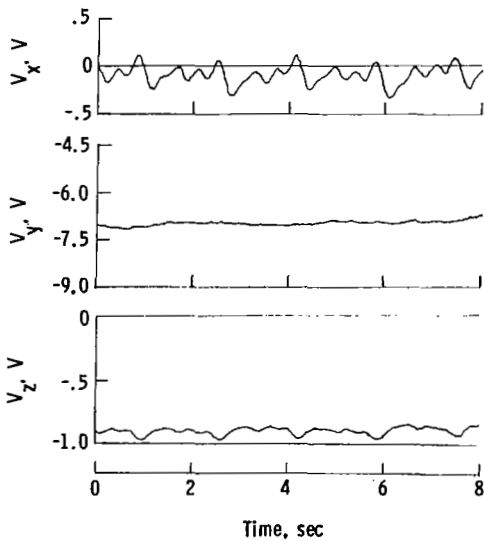


Figure 20.- Time history of signal amplitude in each channel showing ripple caused by concrete reinforcement.

Construction drawings of some sections of Wallops Flight Center runways and taxiways show hook bolts at the transverse joints and three types of longitudinal joints. One type is a saw cut 0.6 cm (0.25 in.) wide and 5 cm (2 in.) deep with continuous reinforcing mesh across the joint. A second type has the same saw cut but with discontinuous reinforcing mesh and dowel bars 2.54 cm (1 in.) in diameter and 45 cm (18 in.) long on 30 cm (12 in.) centers across the joint. A third type is an expansion joint with discontinuous reinforcing mesh and with the same dowel bars across the joint. The heavy dowel bars are located at every third longitudinal joint in some areas and every fourth joint in other areas.

In figure 20 are shown time histories of  $V_x$ ,  $V_y$ , and  $V_z$  taken during a 8.9-m/sec (20-mph) run on the west end of taxiway 10/28 at a displacement of -3.8 m (-12.5 ft). The cable frequency was 990 Hz. The  $V_x$  data exhibit a periodic interference, or ripple, which appears to contain two fundamental frequencies, one being a factor of

three times the other. Analysis of the data reveals that the spatial period of the higher frequency ripple is equal to the length of one concrete section of the taxiway and that the period of the lower frequency ripple is equal to three sections of concrete. Thus, it seems reasonable to conclude that this ripple is produced by distortion of the magnetic field caused by the reinforcing material in the concrete.

Examination of other data reveals that the amplitude of the interference increased as displacement from the cable increased and that the ripple is greater in the  $V_x$  signal than in  $V_y$  and  $V_z$ . Thus the ripple is larger in the  $\hat{\psi}$  output than in the  $\hat{y}_1$  and  $\hat{y}_2$  outputs. Furthermore, the ripple amplitude is significantly less (by a factor of 2 or 3) at 150 Hz and 165 Hz than at 990 Hz. The frequency of the interference changes with the size of the concrete sections and with the speed of the vehicle.

A time history of the  $\hat{y}_1$  and  $\hat{\psi}$  output signals for a run on the south end of taxiway 04/22 is shown in figure 21. These data were taken at 8.9 m/sec at  $y = -7.6$  m (-24.8 ft) and with a current frequency of 990 Hz. Changes in the data are obvious at about  $t = 4$  sec, at which time the van went from a concrete portion of the taxiway to an asphalt portion. Three effects are noticeable: first, the difference in ripple; second, the transient in the  $\hat{\psi}$  data at the transition; and, third, the change in the average output, or bias. The bias shift in the  $\hat{y}_1$  data was about 1.5 m, whereas the shift in  $\hat{y}_2$  (not shown) was about 0.3 m. From other data it can be seen that this bias shift is greatly reduced when the sensor is closer to the center of the runway; at  $y = 0$ , it was negligible. Also, the shift is less with the cable current frequency at 150 Hz than at 990 Hz.

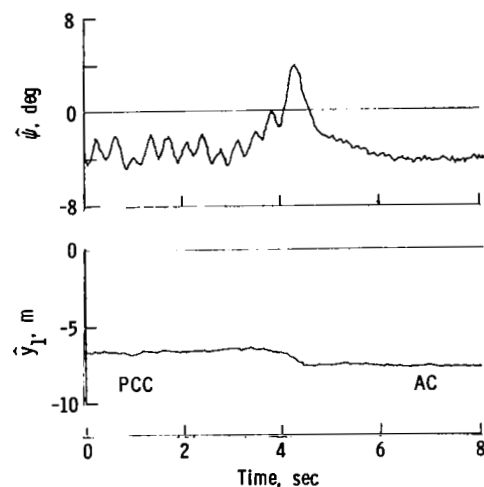


Figure 21.- Time history of sensor output data during transition from concrete to asphalt.

Other transients were detected in the test data. On taxiway 10/28, transients were produced by a drainage culvert located under the taxiway. On taxiway 04/22, some transients appeared to be caused by a wire, or group of wires, crossing under the taxiway.

In summary, the overall effect of the runway construction material, steel mesh, hook bolts, and tie rods, as well as culverts and other metallic material, is to cause spatially correlated noise and bias shifts in the sensor signals. The effect on these signals is less when the sensor is closer to the magnetic leader cable and therefore closer to the desired path. The effects are less at 150 Hz than at 990 Hz.

#### Effect of Aircraft Structure

Prior to the field tests of the sensor system, concern was expressed over the possible effects of the metal in the aircraft structure and skin on sensor performance. This concern was increased by data taken during the van tests at Wallops.

As described previously, the  $\hat{\psi}$  measurement appeared to be significantly affected by the metal in the van even though the coils were located on the support structure several feet from the van itself. The question arose as to whether any sensor measurements could be obtained with the coils located inside a metal enclosure, such as would be true in certain aircraft installations. In an effort to get quick data relative to this question, an aircraft skin simulator - an aluminum cubical box open on two opposing sides - was fabricated. The objective was to obtain data with the coils inside an aluminum structure not to accurately simulate an aircraft installation. The simulator was mounted on the van support structure, and the coils were mounted inside the simulator. Data taken with this arrangement are plotted in figure 22. At 990 Hz, the data exhibit the same strong dependency on  $y$  as before, but there is only a small dependency on  $\psi$ .

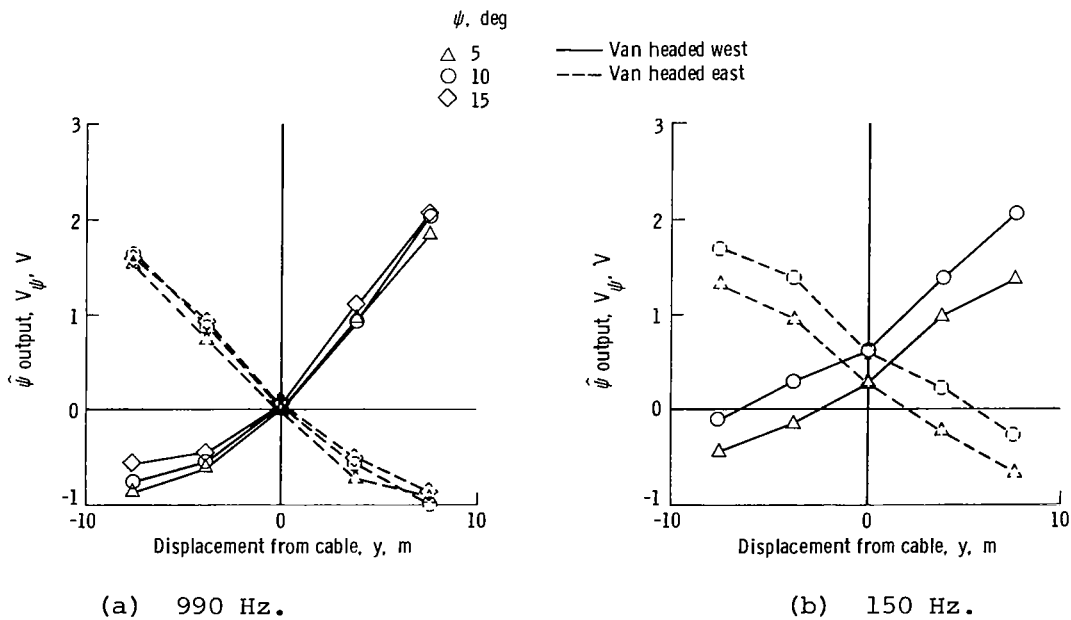


Figure 22.- Static heading data taken with coils inside aircraft skin simulator.

Because of these problems with the  $\hat{\psi}$  data, it seemed advisable to obtain some preliminary data by using a realistic aircraft installation even though a flight-qualified sensor was not available. Therefore, some static data were taken on a taxiway at Langley Research Center with the coils temporarily mounted in the 737 aircraft as described in a previous section. Data taken with the coils mounted in the aircraft nose are plotted in figure 23. The 990-Hz data and the 150-Hz data are very similar; for both sets, the output voltage is a strong function of  $y$  but only a weak function of  $\psi$ . In figure 24 data are plotted for a configuration in which the coils are mounted on a wooden strut protruding below the fuselage from the front end of the nose-wheel well. Once again there is little difference between performance at 990 Hz and 150 Hz. The output is essentially a measurement of  $y$  and is almost independent of the heading  $\psi$ .



To this point, the effects of the aircraft metal structure have been discussed only in relation to the  $\hat{\psi}$  output. The  $\hat{y}_1$  and  $\hat{y}_2$  output data taken with the coils in the aircraft nose are plotted in figure 25. Also shown are similar data with the coils mounted on the van in the usual configuration. Although there are some differences in the aircraft data and the van data, there is sufficient agreement to warrant continuation of the experiment. Both outputs are smoothly varying functions of  $y$ . Whether each aircraft installation would require an individual calibration is an open question.

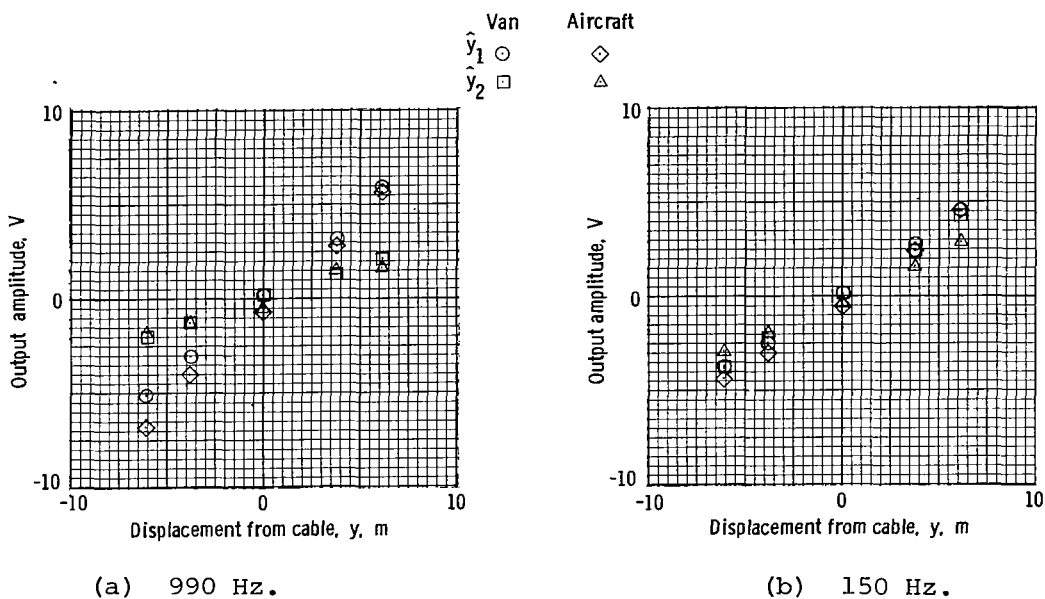


Figure 25.- Static displacement data taken with coils in nose of Boeing 737 aircraft.

In summary, results of tests to date indicate that the sensor might be capable of measuring the displacement of an aircraft from center line but that the sensor might not be useful for measuring aircraft heading because of the distortion of the magnetic field by the metal aircraft.

#### Effect of Electromagnetic Interference

When the sensor was operated with a cable current frequency of 165 Hz, the signals in the three channels at the band-pass filter outputs (fig. 4) prior to detection appeared to be modulated; that is, the waveform looked like an AM signal. The level of modulation was dependent on van position, and the frequency of the modulation was about 15 Hz. While observing the waveform on an oscilloscope, the frequency of the cable current was adjusted. As the cable frequency approached 180 Hz, the modulation frequency approached 0 to indicate that the signal was interacting with a 180-Hz interference, presumably the third harmonic of the 60-Hz primary power. As a direct result of this problem, a test frequency of 150 Hz was selected to replace the test frequency of 165 Hz. This change made the filtering problem simpler, and the modulation effect was almost eliminated.

After the problem of intermodulation with 180 Hz was noticed, a test was conducted to determine the effect of primary power for the runway and taxiway lights on sensor performance. A set of static data was taken on Wallops taxiway 04/22 at various values of  $y$  with the taxiway lights on and with the lights off. A portion of these data is plotted in figure 26. The results show that, at both 150 Hz and 990 Hz, the effect on the measurement  $\hat{y}_1$  of displacement is insignificant near the center line ( $y = 0$ ) but increases nearer the edge of the taxiway. At  $y = -9.45$  m (-31 ft), which was about 2 m from the edge, the  $\hat{y}_1$  output decreased by about 50 percent with the lights on when operating at 990 Hz. The decrease at 150 Hz was much smaller. Though not shown in figure 26, the effect on the  $\hat{y}_2$  output was similar. Although it is encouraging that the effect of taxiway lights was small near the center line, the effect of center-line lights is unknown, since center-line lights are not installed at Wallops Flight Center.

While tests were being conducted at Wallops, there were occasions when the AN/ARS-7 radar was operating within several hundred meters of the test van. Some slight pulsed interference was observed in the  $V_x$ ,  $V_y$ , and  $V_z$  signals, but no effect on the  $\hat{y}_1$ ,  $\hat{y}_2$ , and  $\hat{\psi}$  measurements was detected.

The presence of the various forms of interference, particularly the intermodulation with 180 Hz, raised concern regarding a potential problem with interference from other aircraft electrical systems. To obtain initial data relative to this question, some data were obtained by using the 737 aircraft and the test configuration previously described in the discussion of aircraft metal effects in the preceding section. With the coils located in the nose of the 737, data were recorded on magnetic tape as various aircraft electrical and avionics systems were turned on. Power to the aircraft systems (not the magnetic leader cable sensor) was supplied by the aircraft APU. The data in table II show that the output voltages  $V_{y1}$  and  $V_{y2}$  changed by an order of magnitude or more when the two aircraft busses were switched on. A cable current frequency of 990 Hz and the wide-band filters ( $Q = 0.8$ ) were being used. When narrow-

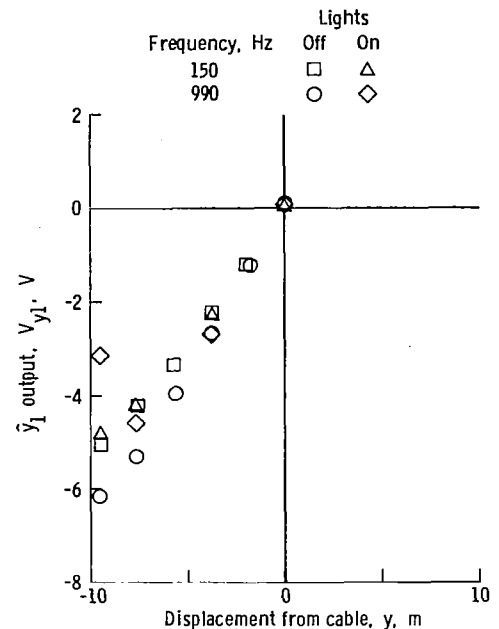


Figure 26.- Static  $\hat{y}_1$  data showing effect of taxiway lights.

TABLE II.- EFFECTS OF AIRCRAFT ELECTRICAL SYSTEM INTERFERENCE ON SENSOR OUTPUT SIGNALS AT 990 Hz

Output signal	Wide-band filter ( $Q = 0.8$ )		Narrow-band filter ( $Q = 5$ )	
	APU on	Busses on	APU on	Busses on
$V_{y1}$ , V . . . .	3.5	-0.2	3.2	2.4
$V_{y2}$ , V . . . .	1.6	-.16	1.6	1.3

band filters ( $Q = 5$ ) were used, the effect was much smaller but still significant. As other avionics were turned on, further changes in the signal levels were observed, particularly with the wide-band filter. One of the largest changes occurred when the weather radar and radar transponder were turned on. However, when a cable current frequency of 150 Hz and a filter  $Q$  of 3 were used, the change in the signals was almost undetectable when the avionics were switched on.

Results of limited testing indicate that sensor performance can be prohibitively affected by interference from other aircraft electrical systems but that it may be possible to reduce these effects to an acceptable level by proper filtering and/or selection of cable frequency. Additional tests in a flight configuration are required to determine the extent of the interference in an optimized sensor system.

### Effect of Band-Pass Filter Phase Response on Synchronous Detector

As previously described, the signals in the x- and z-channels are half-wave detected with synchronous detectors driven by the amplified and limited y-channel signal in order to preserve the relative algebraic sign of the signals. For the correct signal magnitude to be obtained from these detectors, the signal (say, for example,  $v_3(t)$ ) and the reference  $v_2(t)$  must have a relative phase of either  $0^\circ$  or  $180^\circ$ .

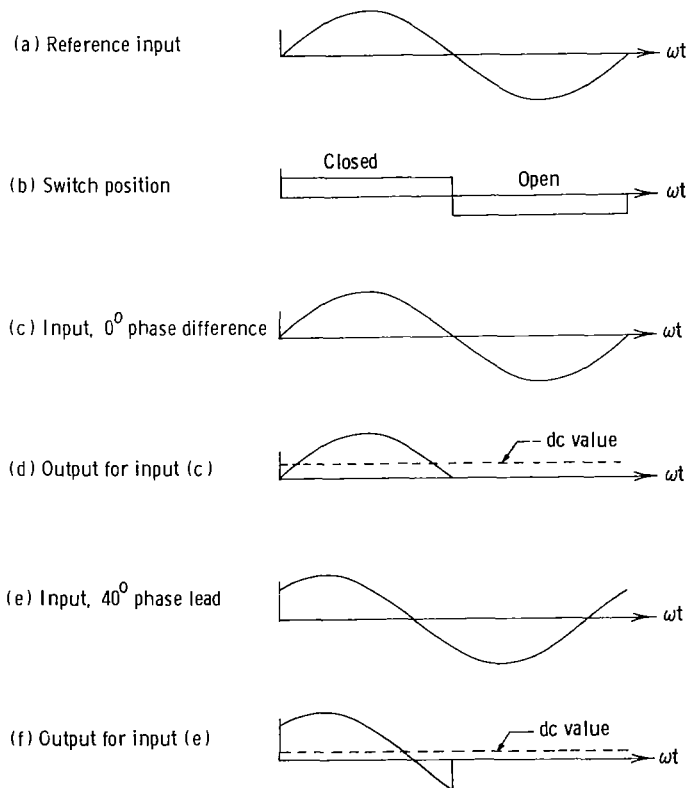


Figure 27.- Synchronous detector waveforms.

In figure 27, waveforms are shown for the signal  $v_3(t)$  leading  $v_2(t)$  by a  $40^\circ$  angle. The output  $v_o$  of the low-pass filter following the rectifier is given by

$$v_o = \frac{1}{2\pi} \int_0^\pi E_3 \sin(\omega t + \beta) d(\omega t) = \frac{E_3 \cos \beta}{\pi} \quad (14)$$

where  $\beta$  is the phase difference. Thus, the magnitude of the output is reduced by the factor  $\cos \beta$  if the relative phase is other than  $0^\circ$  or  $180^\circ$ .

In the experimental system, such undesired phase shifts were introduced by non-matching band-pass filters in the three channels. This effect was particularly noticeable for the relatively narrow-band filters ( $Q = 5$ ). If reduction of interference requires the use of higher  $Q$  filters, more care must be taken in the design and fabrication of the filters than was used in fabricating the experimental system, which was built with parts having tolerances of 5 to 20 percent.

#### Earth Return Tests

A rectangular loop cable configuration requires space to lay the return wire and causes the calibration curves to be nonlinear, as previously described. A potential alternative to a closed loop is to use the earth as the current return path. The first step in investigating this alternative was to measure the circuit resistance of a ground return configuration. A circuit, consisting of three ground rods on each end of a 305-m (1000-ft) leader cable, was installed at the Langley Research Center. The copper clad steel ground rods were 2 1/2 m (8 ft) long and 1/2 cm (5/8 in.) in diameter. This site was relatively low in elevation with wet soil. The resistance in the frequency range from 100 Hz to 2000 Hz was measured to be between 6 and 11  $\Omega$ , and from these results it appeared desirable to conduct further tests at Wallops.

A similar earth return leader cable circuit was installed at Wallops on taxiway 10/28 using two rods on each end of a 306-m (1005-ft) cable shown in figure 10. The soil appeared sandy and dry, and the resistance of this circuit measured between 136 and 140  $\Omega$ . With this resistance the 2-A cable current used for tests at 150 Hz could not be obtained with the experimental equipment because of voltage limitations. The 0.25-A current at 990 Hz could be produced, and some static data were taken with the test van. The  $V_{y1}$  and  $V_{y2}$  data are plotted in figure 28 where it can be seen that the data are not quite symmetrical about the origin; this indicates perhaps that the ground return current density was not symmetrical about the cable.

These tests have neither proved nor disproved the possibility of using an earth return circuit, but the tests do show that an improved grounding technique is necessary. At 990 Hz, the earth return configuration performed well.

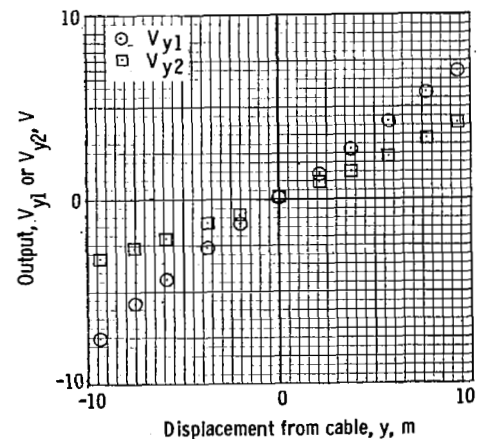


Figure 28.— Static data taken with earth return circuit at 990 Hz.

## Bias and Noise Errors

For each data run, the intent was to compute the sample mean and the sample standard deviation of the error in each of the sensor output variables ( $\hat{y}_1$  and  $\hat{y}_2$ ). These computations were performed by using the following procedure. The data recorded as output voltages were converted to engineering units by using a single-point calibration. This was accomplished by making a static measurement of the output voltages (for example,  $V_{y1}^0$ ) at the intended path distance ( $y^0$ ) and then by calculating the conversion factors ( $y^0/V_{y1}^0$  in m/V) for that run. This calibration measurement was normally made immediately before or immediately after the run, and this procedure amounted to using a different straight-line calibration for each run.

To obtain a true measure of the error in the sensor  $\hat{y}_1$  and  $\hat{y}_2$  outputs would require that the true coil displacement  $y$  be obtained from the recorded TV data for each data sample. The error  $\epsilon_{y1}$  would be calculated as  $\epsilon_{y1} = \hat{y}_1 - y$  for each data sample, and the mean and standard deviation of  $\epsilon_{y1}$  would be computed. A similar procedure would be followed to compute the statistics of the error in  $\hat{y}_2$ . Obviously, this procedure represents an impractical data-processing task. Therefore, approximations of the mean and standard deviation were calculated as follows. For each run, after conversion of the outputs to engineering units by using the single-point calibration, the sample mean and standard deviation of each output were computed. The standard deviation of the output was then taken to be the standard deviation of the error. To get bias error the intended value  $y^0$  was subtracted from the sample mean. There were two significant problems associated with using these bias errors as true indications of sensor performance. First, by subtracting  $y^0$  from the sample mean to get the bias error one assumes that the van was driven along the desired path with zero mean error. Next, using a new calibration measurement for each run eliminates bias errors caused by runway construction differences and by sensor changes due to time, temperature, and other factors.

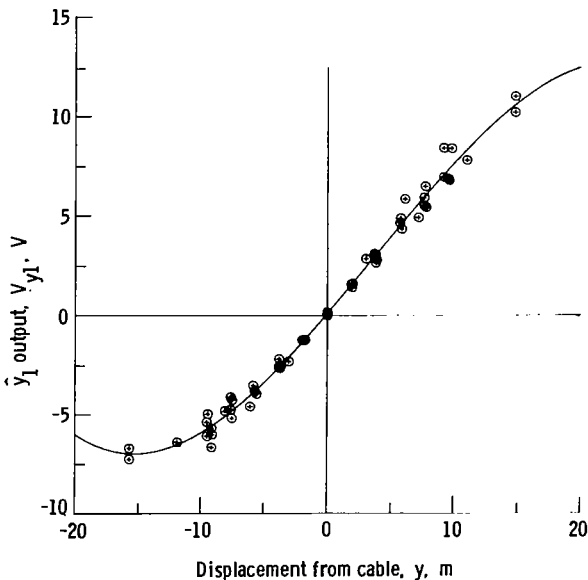


Figure 29.- Calibration curve for  $\hat{y}_1$  at 990 Hz resulting from least-squares fit of polynomial to combined static data.

In order to take some of these factors into account and thus get a more accurate indication of true bias error, further analysis of the static data was performed. The static data at 990 Hz were combined into a single batch, and a least-squares fit using a fourth-order polynomial was performed to obtain a calibration curve (one for  $\hat{y}_1$  and one for  $\hat{y}_2$ ) as a function of  $y$ . The error associated with each static data point was calculated and converted to engineering units by the resulting calibration curve. This process was repeated for the 165-Hz data and the 150-Hz data. A third-order polynomial was also tried, and the differences between the residuals for the third and fourth order were small.

The resulting calibration curve (polynomial) for  $V_{y1}$  at 990 Hz is plotted in figure 29 and is given by the empirical equation

$$V_{y1} = a_0 + a_1 y + a_2 y^2 + a_3 y^3 + a_4 y^4 \quad (15)$$

where

$$a_0 = 0.1115 \text{ V}$$

$$a_1 = 0.7507 \text{ V/m}$$

$$a_2 = 0.007697 \text{ V/m}^2$$

$$a_3 = 0.7207 \times 10^{-3} \text{ V/m}^3$$

$$a_4 = 0.2226 \times 10^{-6} \text{ V/m}^4$$

Also plotted in figure 29 are the  $V_{y1}$  static data at 990 Hz (circles). The residuals, that is, the difference between the calibration curve and each static data point, are plotted in figure 30 after conversion to engineering units for the 990-Hz frequency. Each of these points can be interpreted as a bias error that would

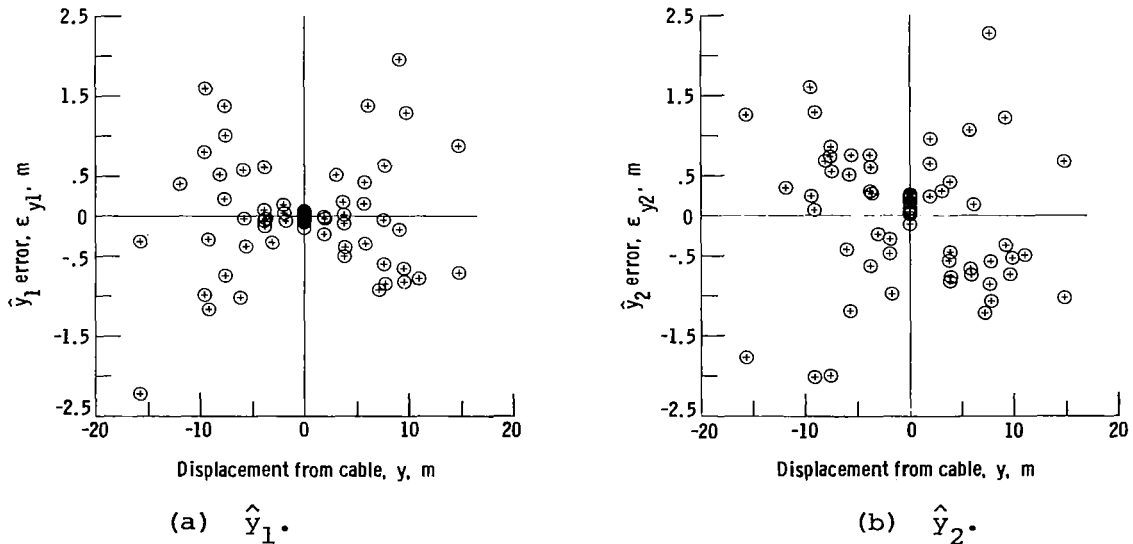


Figure 30.- Residuals from least-squares fit of polynomial to 990-Hz data.

be present in the sensor output for a given runway (or runway segment if the runway has segments of different construction) for that distance from the center line (value of  $y$ ). The residuals for  $\hat{y}_1$  and  $\hat{y}_2$  at 150 Hz are shown in figure 31. It is significant that all these residuals exhibit a smaller bias error near the center line, where the error is generally less than 0.3 m. Also, the  $\hat{y}_1$  residuals are significantly smaller at 150 Hz than at 990 Hz. The reason for this difference is not known but may be because runway construction material has less effect at 150 Hz.

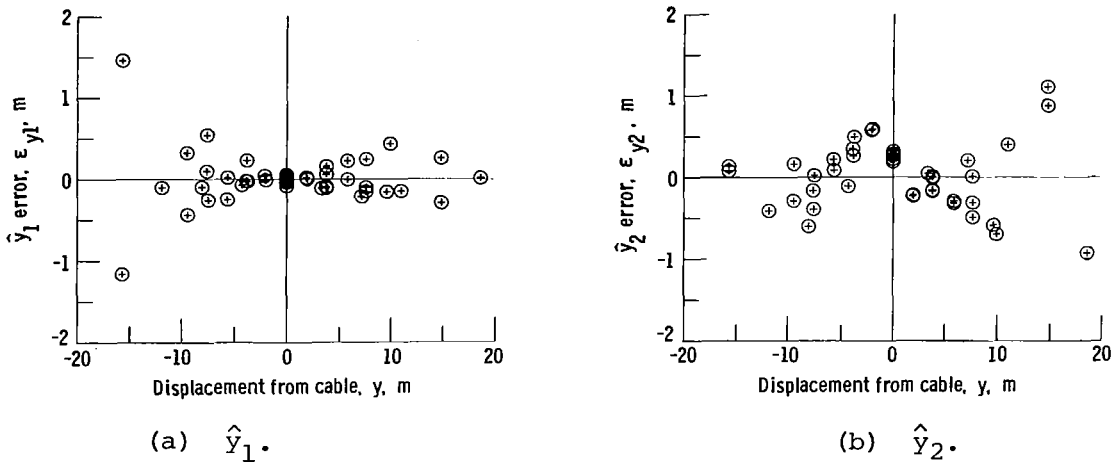


Figure 31.- Residuals from least-squares fit of polynomial to 150-Hz data.

A similar problem exists in interpreting the sample standard deviations as noise error. For the sample standard deviations to be reliable, indicators of noise error would require that the van be driven along the intended path with zero error or at least with negligible error. Examination of the recorded TV data indicates that this was not always true. Rough estimates of the standard deviation of the driving error for several runs ranged from a low of 2 cm to a high of 7.5 cm. Because the driving error is small, these sample standard deviations are useful as indicators of an upper bound on the true standard deviation of the error.

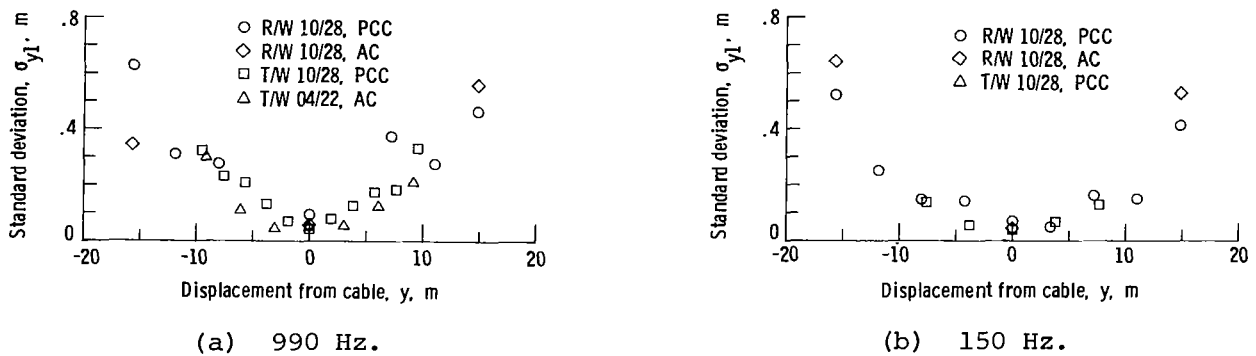


Figure 32.- Standard deviation of the error in dynamic data runs.

Sample standard deviations are plotted in figure 32 for a number of data runs at different test installations at Wallops. Note that at both 150 Hz and 990 Hz, the noise error decreases near center line to less than 15 cm. It should be recalled that these errors include not only driving error but also the effects of amplifier noise, interference, ripple due to concrete reinforcement, support structure vibration, and calibration changes due to the ends of the cable loop. Nonetheless, the noise errors out to 12- or 15-m displacement appear to be small enough for the sensor to be useful, but of course this conclusion must be verified by simulation and test.

## CONCLUDING REMARKS

Comparison of the test data with the theoretical results obtained in NASA Technical Paper 1978 shows good agreement between the theory for a rectangular loop and the performance of the experimental system. Test results show that the sensor is potentially useful as a device for measuring the lateral displacement of an aircraft from its desired path during roll-out and turnoff. Primarily because of distortion of the magnetic field by the metal in the aircraft, the sensor is probably unfit for use in measuring the aircraft heading angle.

The two algorithms used by the sensor to compute lateral displacement require either knowledge of the cable current or knowledge of the sensor coil height. In the tests, both algorithms generally produced decreasing errors with decreasing displacement, and the error was smallest near the desired path (the cable) where accuracies on the order of 0.1 or 0.2 m were achieved. The data taken to date are inconclusive as to which algorithm is better.

The body of the aircraft and the body of the van distorted the magnetic field and introduced errors in the sensor measurements. The measurements of displacement were affected much less than the measurements of heading. The metal reinforcing material in the concrete runways and taxiways introduced a periodic noise in the outputs of the sensor, and transitions from one type of construction to another introduced a bias into the displacement measurement.

Electromagnetic interference from the aircraft electrical systems produced a significant effect on sensor outputs, particularly when operating at 990 Hz. Decreasing the filter bandwidths in the sensor decreased these effects considerably. However, additional testing is required.

The experimental sensor was designed to use two frequencies, 165 Hz and 990 Hz. Performance at 165 Hz was degraded because of interference at 180 Hz, most likely originating from the 60-Hz power frequency. Shifting the lower test frequency to 150 Hz greatly reduced that interference.

The effects of the aircraft metal, the concrete reinforcing material, and other aircraft electrical systems were less with the cable current at 150 Hz, whereas the coil gain was greater and the 180-Hz interference was less with the cable current at 990 Hz. The selection of a frequency could not be determined from the test results, and further experimentation is required to determine the best frequency, whether 150 Hz, 990 Hz, or another frequency as yet untried.

The use of a grounded, or earth, return instead of a return wire may not be practical because the voltage required to drive the current through the cable may be excessive.

Results of the van tests and limited aircraft tests show that the magnetic leader cable system is potentially usable as a sensor to measure aircraft lateral displacement from center line, but additional experimental evaluation is required.

Langley Research Center  
National Aeronautics and Space Administration  
Hampton, VA 23665  
November 9, 1982

## REFERENCES

1. Hammond, A. F.: Guidance and Control of Aircraft Ground Movement at Airports During Restricted Visibility - A Survey of Requirements and Possible Systems. Tech. Rep. No. 65071, British R.A.E., Mar. 1965.
2. Morgan, H. C.; and England, P.: A Taxi-Guidance System for Aircraft Using a Single Magnetic Leader Cable. Tech. Rep. No. 66065, British R.A.E., Feb. 1966. (Available from DTIC as AD 800 204.)
3. Pines, S.; Schmidt, S. F.; and Mann, F.: Automated Landing, Rollout, and Turnoff Using MLS and Magnetic Cable Sensors. NASA CR-2907, 1977.
4. Pines, Samuel: Terminal Area Automatic Navigation, Guidance, and Control Research Using the Microwave Landing System (MLS). Part 1 - Automatic Rollout, Turnoff, and Taxi. NASA CR-3451, 1981.
5. Bundick, W. Thomas: Effects of Cable Geometry and Aircraft Attitude on the Accuracy of a Magnetic Leader Cable System for Aircraft Guidance During Rollout and Turnoff. NASA TP-1978, 1982.

1. Report No. NASA TP-2092	2. Government Accession No.	3. Recipient's Catalog No.	
4. Title and Subtitle RESULTS FROM TESTS, WITH VAN-MOUNTED SENSOR, OF MAGNETIC LEADER CABLE FOR AIRCRAFT GUIDANCE DURING ROLL-OUT AND TURNOFF		5. Report Date January 1983	6. Performing Organization Code 534-04-13-54
		8. Performing Organization Report No. L-15482	10. Work Unit No.
7. Author(s) James C. Young, W. Thomas Bundick, and Stewart H. Irwin		11. Contract or Grant No.	
9. Performing Organization Name and Address NASA Langley Research Center Hampton, VA 23665		13. Type of Report and Period Covered Technical Paper	
		14. Sponsoring Agency Code	
12. Sponsoring Agency Name and Address National Aeronautics and Space Administration Washington, DC 20546		15. Supplementary Notes	
16. Abstract  Tests were conducted with a van-mounted experimental magnetic leader cable sensor to evaluate its potential for measuring aircraft displacement and heading with respect to the leader cable during roll-out and turnoff. Test results show that the system may be usable in measuring displacement but the heading measurement contains errors introduced by distortion of the magnetic field by the metal van or aircraft.			
17. Key Words (Suggested by Author(s)) Magnetic leader cable      Automatic Aircraft guidance          turnoff Avionics Roll-out Aircraft control systems		18. Distribution Statement Unclassified - Unlimited  Subject Category 06	
19. Security Classif. (of this report) Unclassified	20. Security Classif. (of this page) Unclassified	21. No. of Pages 37	22. Price* A03